For submission: https://mc.manuscriptcentral.com/cjoc
For published articles: https://onlinelibrary.wiley.com/journal/16147065

Report

Cite this paper: *Chin. J. Chem.* **2021**, *39*, XXX—XXX. **DOI: 10.1002/cjoc.202100XXX**

New Quinoxaline-Based Blue Emitters: Molecular Structures, Aggregation-Induced Enhanced Emission Characteristics and OLED Application

Xiaoyu Mao,[#a] Fuli Xie,[#b] Xiaohui Wang,[a] Qingsong Wang,[a] Zhipeng Qiu,[c] Mark R. J. Elsegood,[d] Jie Bai,[a] Xing Feng,[*,a] Carl Redshaw,[e] Yanping Huo,[*,c] Jian-Yong Hu,[*,b] Qing Chen[*,f]

[a] *Guangdong Provincial Key Laboratory of Functional Soft Condensed Matter, School of Material and Energy, Guangdong University of Technology, 510006, Guangzhou, P. R. China.*
[b] *Shaanxi Key Laboratory for Advanced Energy Devices, School of Materials Science and Engineering, Shaanxi Normal University, Xi'an 710119, P. R. China.*
[c] *School of Chemical Engineering and Light Industry, Guangdong University of Technology, Guangzhou 510006, P. R. China.*
[d] *Chemistry Department, Loughborough University, Loughborough, LE11 3TU, UK.*
[e] *Department of Chemistry, University of Hull, Cottingham Road, Hull, Yorkshire HU6 7RX, UK.*
[f] *Chinese Research Academy of Environmental Sciences, No.8, Dayangfang, Beiyuan, Beijing, P. R. China.*

Keywords

Quinoxaline | Pyrene | Blue emitter | Aggregation-induced emission | Organic light-emitting diode

Main observation and conclusion

Three new, deep blue light emitters, containing quinoxaline with differing substitution positions (1- or 2- position) pyrene (biphenyl) moieties, were synthesized by a Pd-catalysed coupling reaction in high yield, and were fully characterized by $^{1}H/^{13}C$ NMR spectroscopy, single crystal X-ray diffraction, and high-resolution mass spectrometry (HRMS). The designed molecules exhibited good thermal stability (Tg > 452 °C). Single crystal X-ray diffraction indicated that the compounds containing pyrene units exhibiting π-π stacking, and thus this family of compounds exhibited intramolecular charge transfer (ICT) and non-typical and aggregation-induced enhanced emission (AIEE) characteristics possessing blue emission both in solution and in the aggregation (solid) state. Furthermore, a selected deep blue emitter was utilized as the emitting layer for the fabricating of doped OLED devices, which afforded a deep blue electroluminescence (EL) peak at 428 nm with a narrow FWHM of 57 nm, and the Commission Internationale de L'Eclairage (CIE) chromaticity coordinates of (0.15, 0.06).

Comprehensive Graphic Content

*E-mail: hyxhn@sina.com (X. Feng), hujianyong@snnu.edu.cn (J.-Y. Hu), yphuo@gdut.edu.cn (Y. Huo) and chen.qing@craes.org.cn (Q. Chen)

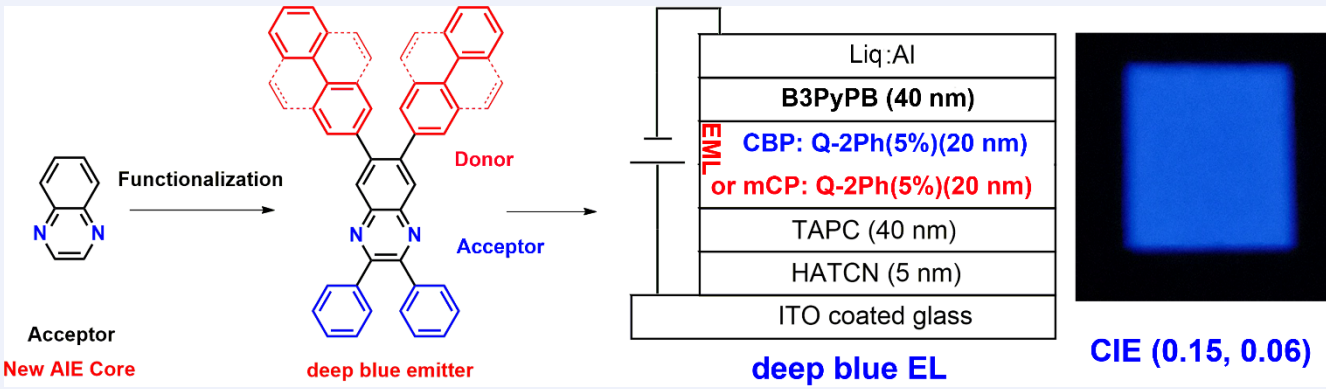

The development of novel π-conjugated organic materials has attracted increasing attention from both the academic and commercial fields, due to their potential application in organic light-emitting diodes (OLEDs,[1-3] organic field-effect transistors (OFETs),[4] organic photovoltaic devices (OPVs),[5,6] biomarkers[7] and biosensors, etc.[8-11] Recently, key points for OLED devices have been explored including the use of high-performance solid-state luminescent materials exhibiting the pure colors of RGB. Stable emission properties for blue emitters are vital for the fabrication of high-performance blue OLED devices, as well as full color-flat displays.[12-14] On the other hand, traditional dyes generally exhibit the concentration/aggregation-caused quenching (ACQ) effect, which greatly limits their use in high technological applications in the solid state.[15,16] Thus, how to enhance emission in the condensed state is a key issue in the field of luminescent materials.

Tang *et al*. observed that hexaphenylsilole (HPS) shows non-emission in solution but enhanced emission in the aggregated or solid-state, and defined this abnormal photophysical phenomenon as aggregation-induced emission (AIE) back in 2001.[17] The working mechanism of AIE was explained in terms of the restriction of intramolecular motions (RIM). Up until now, many categories of blue emitters with AIE features have been reported for OLED applications,[18-20] but high-performance near-ultraviolet emitters and violet-blue OLEDs with CIEy equal to or less than 0.08 are rare. Recently, Ma *et al*. reported efficient violet-blue AIEgens with a D-A structure, which exhibit a maximum external quantum efficiency of 4.34% with Commission Internationale de L'Eclairage (CIE) coordinates of (0.159, 0.035).[21]

It is noteworthy that nitrogen-containing heterocyclic-based systems open up a new avenue to access N-type AIEgens, which are not only biological materials with good biocompatibility, but can also be used in organic electronics as highly-efficient fluorescent materials.[22-28] For example, tetraphenylpyrazine, bearing electron-withdrawing groups, has attracted considerable attention for the development of new AIEgens, which not only exhibit favorable thermal stability, but also possess efficient color-tunable emission from deep blue to sky blue.[27] Previous reports have indicated that the compound 1,4,5,8-tetraazaanthracene (TAA) is an ACQ chromophore whose core is functionalized at the 2,3,7,8-positions, and the ACQ of TAA can be converted into an AIE luminogen which exhibits tunable color emission from sky blue to red, depending on the substituents.[28] Alternatively, the electron-deficient quinoxaline core is easy to modify for the preparation of highly-efficient functional materials. For example, (*E*)-6-((2-phenylhydrazono)methyl)quinoxaline derivatives displayed superior antifungal and antioxidant activity,[29] while bipolar molecules of quinoxaline compounds exhibit full color fluorescence by arylating at the 5,8-positions of the quinoxalines.[30] More importantly, quinoxaline-based D-A-D molecules displayed high-contrast reversible mechano- and thermo-responsive behavior in the solid state.[31] Grazulevicius and co-workers reported a series of carbazole-quinoxaline-carbazole compounds, which showed thermally activated delayed fluorescence with mechanochromic luminescence properties.[32-33] Moreover, when the carbazole group was replaced by an iminodibenzyl moiety, the quinoxaline-containing iminodibenzyl compounds exhibited an interesting dual thermally activated delayed fluorescence (TADF) as well as room temperature phosphorescence (RTP) properties.[34] Thus, we believed that the quinoxaline unit would be a highly useful scaffold for constructing novel multifunctional materials for organic electronics applications.

In this study, to further explore the photophysical properties of quinoxaline-based derivatives and their potential application in organic electronics, three new 2,3-phenyl-6,7-diarylquinoxalines were synthesized, in order to investigate their AIE characteristics, optical properties, electroluminescent behavior, as well as OLED applications. The pyrene or biphenyl moieties were attached at configuration of the AIE behavior. Due to the presence of the electron-withdrawing quinoxaline unit, the series of compounds **Q-1-Py** and **Q-2-Py** exhibited a strong intramolecular charge transfer (ICT) process and caused a large red-shift in the emission spectrum, where the pyrene units acted as donating groups. The **Q-2Ph** exhibited deep blue emission both in solution and in the solid state with aggregation-induced emission characteristics. More importantly, the compound **Q-2Ph** was selected as a blue emitter for a doped OLED which had CIEy less than 0.06.

Results and Discussion

2 Synthesis and characterization

As shown in Scheme 1, the quinoxaline-based compounds were synthesized with the condensation reaction of benzyl and 4,5-dibromobenzene-1,2-diamine in acetic acid solution under reflux conditions to afford 6,7-dibromo-2,3-diphenylquinoxaline (**1**) in 85% yield. Then, a Suzuki-coupling reaction for **1** and arylboronic acid afforded **Q-1-Py**, **Q-2-Py**, and **Q-2Ph** in considerable yield. The three new compounds were purified by column chromatography, and the high purity compounds **Q-1-Py**, **Q-2-Py**, and **Q-2Ph** were used in OLED device fabrication via vacuum sublimation.

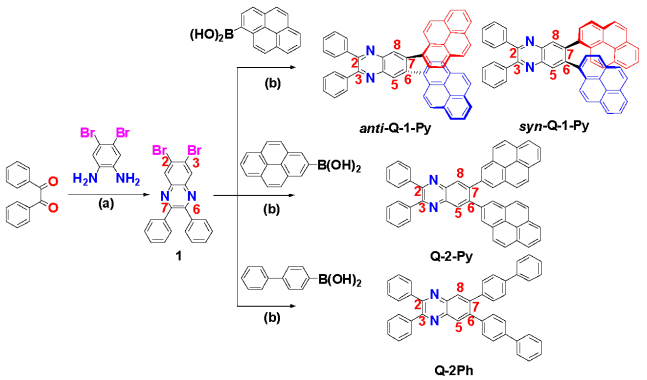

Scheme 1. Synthetic route for the three quinoxaline-based compounds by a Suzuki-Miyaura coupling reaction: (a) acetic anhydride, (b) $Pd(PPh_3)_4$, K_2CO_3, toluene/ethanol/H_2O.

The three compounds were characterized with $^1H/^{13}C$ NMR spectroscopy, single crystal X-ray diffraction analysis, and high-resolution mass spectrometry (HRMS) techniques. In addition, our previous report indicated that when two 1-pyrenyl units reside at the *ortho*-positions of the central phenyl ring, two conformers (*anti*- and *syn*- conformation) are formed.[35] Thus, we suspected that maybe two molecular conformations (*anti*- and *syn*-) are also present in compound **Q-1-Py**. According to the ^1H NMR spectra of **Q-1-Py**, high-performance liquid chromatography (HPLC) analysis might be needed for further purification of the conformers, however, the HPLC results indicated that the **Q-1-Py** exhibited only one peak with a retention time of 18.27 min with M/S = 682.00. This can be ascribed to the pyrene unit freely rotating without steric hindrance at the 5- and 8- positions of the quinoxaline core, leading to interconversion of the *anti*- and *syn*-conformations in solution. All compounds were soluble in common solvents such as dichloromethane, tetrahydrofuran (THF), acetone, and toluene, but insoluble in water. The thermal stability of the quinoxaline-based compounds **Q-1-Py**, **Q-2-Py**, and **Q-2Ph** was investigated by thermo-gravimetric analysis (TGA) and differential scanning calorimetry (DSC) under a nitrogen atmosphere, and the results are shown in Figure S11-S12. The compounds have a slight weight loss of 3.4% (**Q-1-Py**) and 1.3 % (**Q-2-Py**) corresponding to solvent loss, then a large broad endothermic band with an endothermic peak (558 °C for **Q-1-Py**, 581 °C for **Q-2-Py** and 561 °C for **Q-2Ph**), which corresponds to decomposition of the molecular frameworks. Thus, the

compounds **Q-1-Py**, **Q-2-Py**, and **Q-2Ph** exhibited excellent thermal stability with decomposition temperatures (T_d, 5% weight loss) of 493 °C, 527 °C, and 452 °C, respectively. In the DSC thermogram, a single endothermic peak at 315 °C for **Q-1-Py**, 324 °C for **Q-2-Py**, and 296 °C for **Q-2Ph**, corresponding to the melting points. In addition, both compounds possess high glass-transition temperatures (T_g) of 300 °C for **Q-2-Py** and 253 °C for **Q-2Ph**, but the T_g of compound **Q-1-Py** could not be detected.

2 X-ray single crystal diffraction analysis

The 1- and 2-substituted pyrene moieties were introduced into the quinoxaline skeleton to investigate the effect of differing substitution patterns at the pyrene moiety on the molecular packing in the crystalline state. Crystals of quinoxaline-based compounds suitable for single X-ray diffraction analysis were grown by vapor diffusion of *n*-hexane into dichloromethane solution. Their crystal structures are displayed in Figure 1 and the selected crystallographic data are summarized in Table S1.

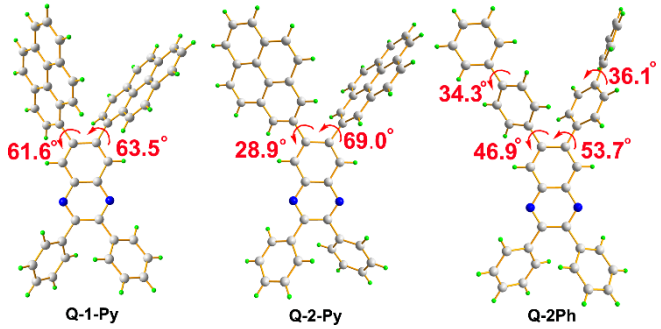

Figure 1. The X-structures of the quinoxaline-based compounds **Q-1-Py**, **Q-2-Py**, and **Q-2Ph**.

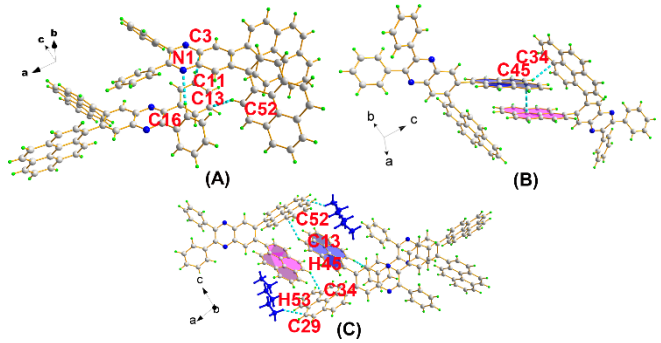

Figure 2 Crystal packing diagrams of compound **Q-1-Py** (A) adjacent compounds connected by several C–H···π interactions, (B) and (C), with π-π stacking interactions.

The compound **Q-1-Py** crystallized in the monoclinic space group $P2_1/c$, and the asymmetric unit contains one molecule of **Q-1-Py** and *ca*. 58% of a hexane molecule, due to probable partial desolvation. Previously, our group reported two pyrene-fused hexaarylbenzene stereoisomers, which exhibited two different molecular configurations (*anti*- and *syn*- configurations), leading to multiple photoluminescence properties.[35] However, we only achieved a *syn*-configuration in compound **Q-1-Py** and the pyrene units were oriented 'up' relative to the quinoxaline rings. The twist angles between the quinoxaline and pyrene units were 61.56(5)° and 63.45(5)°. As shown in Figure 2, the adjacent **Q-1-Py** interacted in a head-to-tail orientation via several weak hydrogen and C–H···π bonds (C11–H11···C3 = 3.31 Å, C16–H16···N1 = 2.56 Å, C52–H52···C13 = 2.90 Å and C45–H52···C13 = 2.80 Å). On the other hand, the neighboring pyrene unit exhibited a slightly slipped π-stacking interaction along the *a*-axis with a centroid-centroid distance of 3.402 Å, indicating a J-aggregation mode in the structure of **Q-1-Py**.[36]

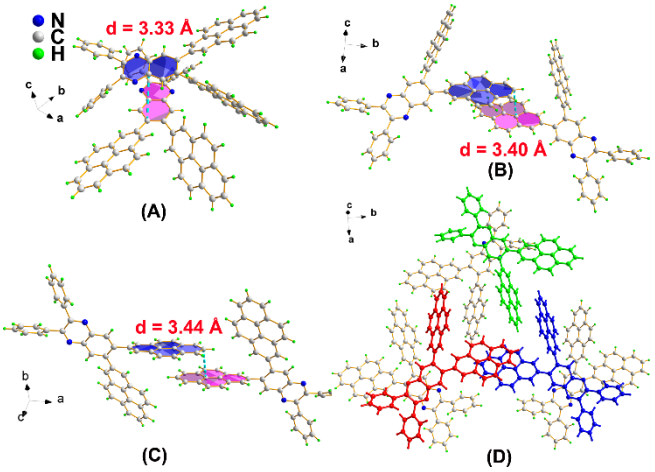

Figure 3. Crystal packing diagrams of compound **Q-2-Py** with (A) π-π stacking interaction patterns by quinoxaline cores crisscrossed along the *c*-axis; π-π stacking by pyrene rings along the (B) *a*- and (C) *b*- axis; (D) self-assembled prism architecture.

The substitution pattern plays a significant role in affecting the molecular packing and opto-electronic properties.[37,38] Indeed, in crystal **Q-2-Py**, when the substituents are at the 2-position of the pyrene unit, the pyrene moiety adopted a propeller twist topology with the dihedral angles between the pyrene rings and quinoxaline core of 28.91(2)° and 69.00(3)°. Although the **Q-2-Py** also crystallized in the monoclinic space group $P2_1/c$, which is the same as **Q-1-Py**, the unit cell was somewhat smaller due to crystallizing without the solvent, and the crystal structure revealed a greater diversity of intermolecular interactions. Three kinds of crystal packing modes were displayed in the crystal structure of **Q-2-Py** (Figure 3). The quinoxaline cores crisscrossed and formed a columnar structure along the *c*-axis by π···π stacking interactions with the shortest contact between N(2) and C(5') = 3.077 Å (Figure 3A). The pyrene moieties adopted two kinds of π···π stacking modes along the *a*- and *b*- axis, (Figures 3B and 3C, respectively). One of the pyrene rings exhibited a co-facial arrangement (H-aggregation) between symmetry-related pyrene rings with the terminal rings overlapping with a centroid-centroid distance of 3.40 Å.[35] A slipped π-stacking interaction was observed between two neighboring pyrene moieties along the *a*-axis (Figure 3C). Further, the three patterns were self-assembled into a regular prism architecture by weak intramolecular interactions (Figure 3D).

2 Photophysical properties

The photophysical characteristics of the target quinoxaline-based compounds were examined by UV-vis absorption and photoluminescence in THF solution (*ca*. 10^{-5} M) and the relevant parameters are summarized in Table 1. Due to the different substitution pattern at the pyrene moiety, the electronic absorption spectra of **Q-1-Py** and **Q-2-Py** displayed different absorption behavior. **Q-2-Py** exhibited a pyrene-like absorption mode and two strong absorption bands located at around 285 and 342 nm with a shoulder peak at 371 nm (Figure 4A),

Table 1. The photophysical and electrochemical properties of the quinoxaline-based compounds

Compd.	λ_{abs}(nm) solns[a]/film	λ_{PL} (nm) solns[a]/film[b]	Φ_f	LUMO (eV)	HOMO (eV)	$\triangle E_g$ (eV)	$Tg/T_m^g/T_d^h$ (°C)
Q-1-Py	346/353	499/501	0.49 (0%) 0.02 (60%)	–1.96[c] (–2.78)[d]	–4.87[c](–5.69)[e]	2.91[c] (2.91)[f]	-/315/ 493

			0.19 (0%) 0.02 (60%)				
Q-2-Py	342/350	472/476	0.09 (70%) 0.15 (99%) 0.08 (film)	–1.96 (–2.56)	–5.28 (–5.55)	3.32 (2.99)	300/324/ 527
			0.16 (0%)				
Q-2Ph	375/382	423/440	0.38 (50%) 0.23 (99%) 0.17 (film)	–1.96 (–2.85)	–5.69 (–5.92)	3.73 (3.07)	253/296 / 452

[a] Maximum absorption wavelength measured in THF at room temperature. [b] Measured in thin films. [c] Calculated by DFT/B3LYP/6-31G* using Gaussian 03 software. [d] LUMO = HOMO + E_g. [e] Determined by CV using ferrocene as reference calculated by the empirical formulae HOMO = − (4.8 + $E_{ox,onset}$ − $E_{ox,onset}$(Fc)). [f] Estimated from UV/Vis absorption spectra. [g] Melting temperature (T_m) obtained from DSC analysis. [h] Decomposition temperature (T_d) obtained from thermo-gravimetric analysis.

which are consistent with the $S_3 \leftarrow S_0$, $S_2 \leftarrow S_0$, and $S_2 \leftarrow S_0$, transitions, respectively.[39] With the substituent at the 1-position in compound **Q-1-Py**, the long-wavelength absorption peak has slightly red-shifted to 346 nm compared with compound **Q-2-Py**, which may be ascribed to the effect of both $S_2 \leftarrow S_0$ and $S_1 \leftarrow S_0$ transitions.[39] For **Q-2Ph**, two well-defined absorption bands at 292 and 375 nm were observed which were assigned to a π - π* transition and an n - π* transition, respectively. The molar extinction coefficients (ε) of the **Q-1-Py** and **Q-2-Py** in THF solution were almost the same and higher than **Q-2Ph**, probably due to the expanding π-conjugation in the molecular frameworks. Additionally, the maximum absorption band showed a slight red-shift (< 10 nm) in the thin film, compared with those in solution (Table 1).

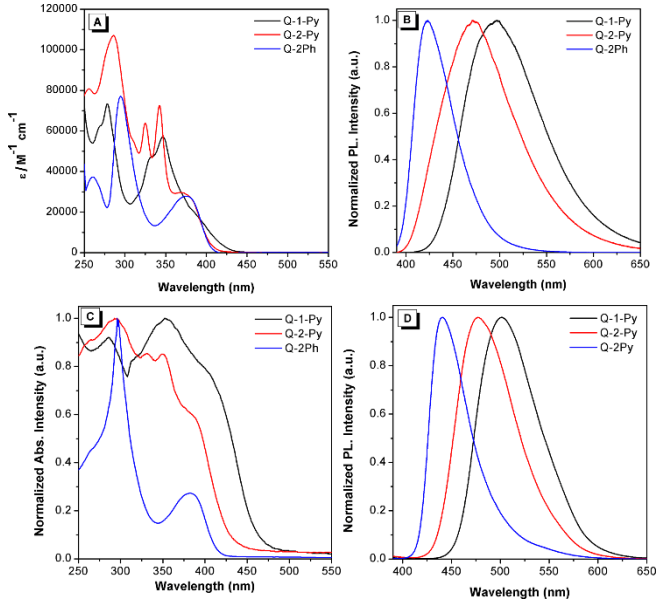

Figure 4. (A) The UV-Vis absorption and (B) emission spectra of the three quinoxaline-based compounds recorded in THF at about 10^{-5} M at room temperature. (C) normalized UV-Vis absorption and (D) emission spectra in thin films at room temperature.

The compounds **Q-2-Py** and **Q-2Ph** emitted intense blue (sky-blue) fluorescence in THF solution with a $\lambda_{max\ em}$ of 472 and 423 nm, respectively. However, the maximum emission peak of **Q-1-Py** was located at 499 nm with a 27 nm red-shift compared with **Q-2-Py**. The different emission behavior can be attributed to the strong electron-withdrawing group of the quinoxaline unit positioned at the 1-position of the pyrene, which influences the $S_1 \leftarrow S_0$ excitation by strong electronic interactions.[39] On the other hand, due to the weak electronic interactions between the 2-substituted pyrene and the quinoxaline units, the fluorescence spectra of **Q-2-Py** still exhibited a similar emission profile as seen for the parent pyrene core.[39-40] The quinoxaline-based compound **Q-2-Py** displayed a blue-shifted emission with a maximum peak at 476 nm in the solid state due to H-aggregation.[41,42] The emission of **Q-2-Py** and **Q-2Ph** displayed a red-shift of *ca*. 10 nm in the emission band in the thin film compared with that in solution, and this may ascribed to strong intermolecular interactions. The FWHM of **Q-1-Py**, **Q-2-Py** and **Q-2Ph** were 45, 74, and 71 nm in the solid state, respectively.

Generally, the pyrene would act as electron-donor or acceptor depending on the micro-environment of the whole molecular structure,[41,43] and the biphenyl units are weak electron-donating groups, while the quinoxaline containing a pyrazine is an electron withdrawing group. Thus, the quinoxaline-based blue emitters would be bipolar molecules. To examine the effect of solvent polarity, the fluorescence of **Q-1-Py**, **Q-2-Py**, and **Q-2Ph** were measured in six kinds of solvents, namely cyclohexane (Cy), tetrahydrofuran (THF), 1,4-dioxane, acetonitrile (ACN), dimethyl sulfoxide (DMSO), and dimethylformamide (DMF). As the solvent polarity increases from Cy to DMF, the maximum emission peaks were red-shifted by *ca*. 123 nm for **Q-1-Py** and 145 nm for **Q-2-Py**, with tunable emissive color from deep blue to yellow, indicating that these quinoxaline-based blue emitters are sensitive to the polarity of the environment due to a strong intramolecular charge transfer (ICT) effect. However, the polarity of the solvent has a limited effect on the absorption behavior of these compounds, due to the similar dipole moments in the ground state and in the Franck-Condon excited-state (LE state).[44-45] Furthermore, the linear relationship of the Stokes shifts (Δv) [Equation (1)] against the solvent parameters was confirmed by the Lippert-Mataga equation, (2).

$$\Delta v = \frac{2\Delta\mu^2}{hcR^3}\Delta f + const \qquad (1)$$

$$\Delta f = \frac{\varepsilon-1}{2\varepsilon+1} - \frac{n^2-1}{2n^2+1} \qquad (2)$$

Δv is the Stokes shift, Δμ was calculated from the difference in the dipole moment of the solute molecule between the excited (μ_e) and ground (μ_g) states, h is Planck's constant, R is the radius of the solvent cavity in which the fluorophore resides (Onsager cavity radius), Δf is the orientation solvent polarity parameter, ε is the static dielectric constant, and n is the refractive index of the solvent and the relative solvent parameters are listed in Table S3.

2 AIE characteristics

Previously, Tang *et al*. reported that tetraphenylpyrazine (TPP) and TAA-containing luminogens exhibited typical AIE characteristics.[15] To inspect the AIE features of the quinoxaline-based blue emitters, their fluorescent behavior (at ~10^{-5} M) was recorded in THF/water mixtures with various water fractions (f_w). Upon excitation, the compounds **Q-1-Py**, **Q-2-Py**, and **Q-2Ph** emitted blue with the maximum emission peaks at 494 nm, 465 nm, and 423 nm in pure THF, respectively. As the water fraction increases to 99%, the compounds underwent opposite optical behavior as observed by naked-eye observation of the visible emission color changes. The compound **Q-2-Py** displayed a bright emission in THF (Φ_f = 0.19), which fully decreased with a large red-shifted emission at 540 nm as the water fraction increased to 60% (Φ_f = 0.02). This process is ascribed to the ICT effect, and as the water fraction increased to over 60%, the emission intensity enhanced again and the emission peak was blue shifted to 471 nm when the f_w = 70% (0.09). This was ascribed to the AIE effect that dominates this process, resulting in an enhanced emission, and then the emission intensity

was quenched due to the molecular aggregation in the aggregation state (f_w = 99%, Φ_f = 0.15). Also, **Q-1-Py** exhibited similar emission behavior to **Q-2-Py** in THF/water mixtures at various water fractions (f_w). On the other hand, the compound **Q-2Ph** exhibited strong deep blue emission (423 nm) in diluted THF solution (Φ_f = 0.16), as the water fraction (f_w = 10%) increased. The emission intensity at 423 nm was quenched directly, which was likely caused by the solvent polarity increasing and the transformation of the ICT effect. As the f_w increased to 50%, the emission intensity was enhanced *ca*. 6-fold with a large red-shift to 454 nm (Φ_f = 0.38), which may be ascribed to the crystallization-enhanced emission.[46] Subsequently, the emission intensity gradually decreased as the f_w increased to 99%, with a blue-shifted emission peak at 434 nm (Φ_f = 0.23). The hydrophobic molecule **Q-2Ph** prefers to form an aggregate at higher f_w, leading to the AIE effect which overwhelms the ICT effect.[47,48]

Further, to remove the ICT effect on the AIEE process, the PL spectra were performed in dichloromethane (DCM) and hexane/DCM mixtures. As shown in Figures S18-20 for the **Q-2-Py** case, as the hexane is added to the DCM solution, the emission peak at 503 nm in DCM was blue-shifted to 419 nm with an enhanced emission intensity in the hexane content of 99%. This result is strong evidence that the **Q-2-Py** is an AIEE-active material, and the solvent polarity also plays a significant role to effect the AIE characterhaistc of quinoxaline-based blue emitters.[49]. Based on the results, the three quinoxaline-based chromophores **Q-1-Py**, **Q-2-Py**, and **Q-2Ph** were blue emitters with both ICT plus AIEE characteristics in the highly polar THF/H_2O mixture, and also exhibit typical AIEE characteristics in the less polar solvent mixture of DCM/hexane.[50]

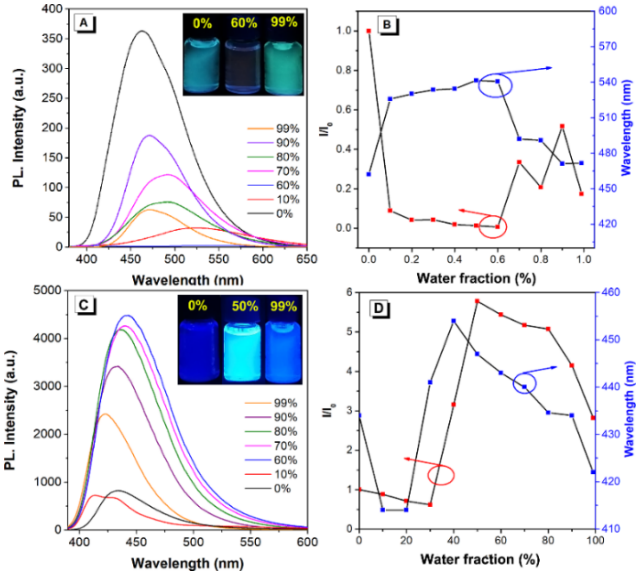

Figure 5 (A) and (C) PL spectra of **Q-2-Py** and **Q-2Ph** in THF/water mixtures at different water fractions (f_w). (B) and (D) Plots of relative PL intensity (I/I_0) *versus* the composition of THF/water mixtures, where I_0 is the PL intensity in pure THF solution. The red squares are for the effect on I/I_0, while blue circles are for the wavelength.

2 Quantum calculations

To understand the electronic structures of the quinoxaline-based blue emitters, density functional theory (DFT) calculations in the gas phase were performed at the RB3LYP/6-31G(d) level, and the structures were correlated according to their single crystal structures. The optimized molecule and the corresponding HOMO-LUMO surfaces of **Q-1-Py**, **Q-2-Py**, and **Q-2Ph** are illustrated in **Figure 6**. The dihedral angles between the quinoxaline core and the two pyrenes in **Q-1-Py** are 58.3° and 71.0°, respectively, and both substituents in **Q-2-Py** and **Q-2Ph** with a quinoxaline core have similar dihedral angles at 51.1 ° for **Q-2-Py** and 50.5 ° for **Q-2Ph**. For **Q-1-Py** and **Q-2-Py**, the HOMO and LUMO levels are almost separated in the pyrene units and in the quinoxaline segments, respectively. The difference was that the majority of the HOMO electron density of **Q-1-Py** was only located in one pyrene unit, and the **Q-2-Ph** was mainly located at both pyrene units. For **Q-2Ph**, the HOMO level spread over the whole molecular skeleton. This difference could be attributed to the presence of large dihedral angles in **Q-1-Py**; the HOMO and HOMO-1 level were separated at the different pyrene units. (Figure S26) Moreover, the LUMO was mostly concentrated on the quinoxaline core in the three quinoxaline-based derivatives. Although the different position-dependent substituents were localized on the 6,7-positions of the quinoxaline core, all the LUMO values were –1.96 eV. On the other hand, the HOMO values increased from –5.69 eV to –4.87 eV as the π-conjugation expanded from **Q-2Ph** to **Q-2-Py** and **Q-1-Py**. The HOMO-LUMO gaps of the compounds **Q-1-Py**, **Q-2-Py**, and **Q-2Ph** were calculated to be 2.91 eV to 3.73 eV. Furthermore, cyclic voltammetry (CV) was performed to investigate the electrochemical properties of the three quinoxaline-based compounds **Q-1-Py**, **Q-2-Py**, and **Q-2Ph**, and the HOMO and LUMO energy levels were derived from the onset of oxidation potential according to the equation, $E_{HOMO} = -(4.8 + E_{oxset} - E_{oxset\ (Fc)})$ eV, and the $E_{LUMO} = E_{HOMO} - E_g$, in which E_g was the optical energy gap (Figure S25). The detailed values are listed in Table 1. The experimental data for the LUMO levels were somewhat lower than from the theoretical calculations.

Table 2. Summary of the electroluminescent performance of the deep blue devices.

	V_{on} (V)	L_{max} (cd/m²)	$\eta_{C,max}$ (cd/A)	$\eta_{p,max}$ (lm/W)	EQE (%)	λ_{max} (nm)	CIE (x, y)
Device I	3.7	266	0.44	0.33	0.90	429	(0.15, 0.06)
Device II	4.0	383	0.82	0.71	0.90	428	(0.15, 0.06)

Device 1: ITO/HATCN(5 nm)/TAPC(40 nm)/CBP: Q-2Ph(5%)(20 nm)/B3PyPB (40 nm)/LiF (1 nm)/Al(100 nm)
Device II: ITO/HATCN(5 nm)/TAPC(40 nm)/mCP: Q-2Ph(5%)(20 nm)/B3PyPB (40 nm)/LiF (1 nm)/Al(100 nm)

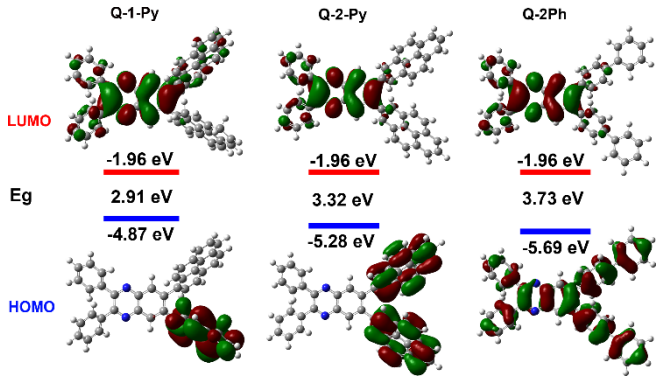

Figure 6. Computed molecular orbital plots (B3LYP/6-31G*) of the three quinoxaline-based compounds; the blue and red in the molecular configuration represent electron density.

2 Electroluminescent Devices

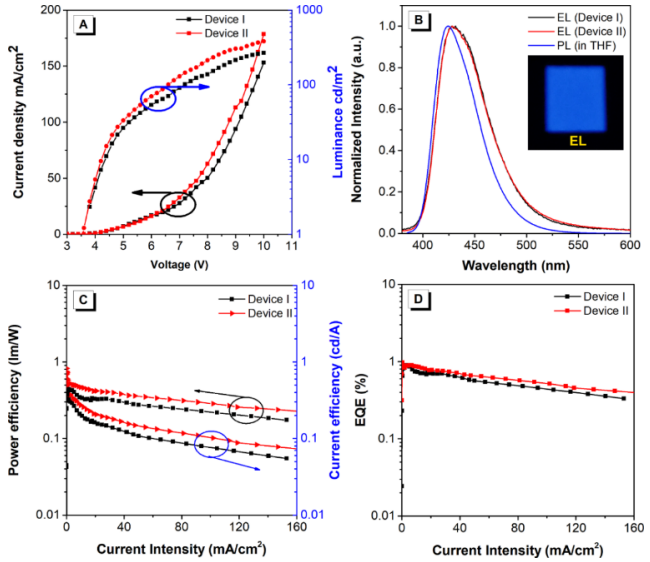

Figure 7. (A) Plot of luminance and current density with the applied voltage, (B) EL spectra, (C) plot of current density *versus* power/current efficiency curve and (D) the current density *versus* external quantum efficiency.

Due to its high thermal stability and blue emissive properties with a considerable quantum yield, the AIEE luminous **Q-2Ph** was selected as the emitting layer (EML) for further electroluminescent studies. Two different types of multilayer OLED devices were fabricated with the following configuration: ITO/HTACN/TAPC/EML (CBP or mCP:Q-2Ph)/B3PyPB/LiF/Al, where the 1,4,5,8,9,11-hexa-azatriphenylenehexacarbonitrile (HATCN) and 4,4'-cyclohexylidenebis [*N*,*N*-bis(4-methylphenyl) benzenamine] (TAPC) were adopted as hole-transporting layers (HTL), while 1,3-bis(3,5-dipyrid-3-ylphenyl)benzene (B3PyPB) was used as the electron-transporting layer (ETL). The electroluminescent spectra, current density-voltage-luminance (J-V-L) characteristics and the external quantum efficiencies of the devices are illustrated in Figure 7, and the device parameters are summarized in Table 2. Both doped OLEDs exhibited a deep blue emission (429/428 nm) with a narrow FWHM of 57 nm, and a considerable external quantum efficiency (EQE) of 0.9 %. More importantly, the doped-device II exhibited a relatively high brightness (L), luminance efficiency, and power efficiency current of 383 cd m^{-2}, 0.82 cd A^{-1} and 0.71 lm W^{-1}, respectively, compared with the doped device I.

2 pH effect

Previously, Tang *et al*. reported that 1,2-dihydroquinoxaline derivatives exhibited an AIEE characteristic for the highly sensitive detection of biogenic amines.[51] Thus, the pH effect for these quinoxaline-based blue emitters was investigated. The fluorescence spectra indicated that the emission behavior of these three compounds **Q-1-Py**, **Q-2-Py**, and **Q-2Ph** in THF solution (10^{-5} M) exhibited only limited change as the pH value was changed from 1 to 14. However, when fumed with HCl vapor for about 10 s, the emission peak of a thin film of **Q-2Ph**, located at 430 nm, decreased and this was accompanied by a new yellow emission peak arising at 544 nm (Figure 8). The blue emission was restored to 430 nm in a NH_3 environment. Furthermore, this conversion of emission behavior from blue to yellow could be repeated more than 20 times without fatigue, and the larger, red-shifted emission may be attributed to strong intramolecular charge transfer by a protonated quinoxaline section in the HCl vapor. In contrast, for compounds **Q-1-Py** and **Q-2-Py**, no new emission peak was observed in HCl or NH_3 environments. Due to the presence of the N atom in the core, the electron-deficient quinoxaline would be protonated, leading to an enhanced electron pull-push ability and in turn strengthens the ICT character and achieves a large, red-shifted emission. While for **Q-1-Py** and **Q-2-Py**, the expanded π-conjugation of the pyrene unit would delocalize the electron, resulting in a related low electron pull-push ability compared with the diphenyl units. Thus, when protonation of both **Q-1-Py** and **Q-2-Py** took place, we observed a decreased in the emission intensity (Figure S27-S28).[52-53]

[a] *Department, Institution, Address 1*
E-mail:

[b] *Department, Institution, Address 2*
E-mail:

[c] *Department, Institution, Address 3*
E-mail:

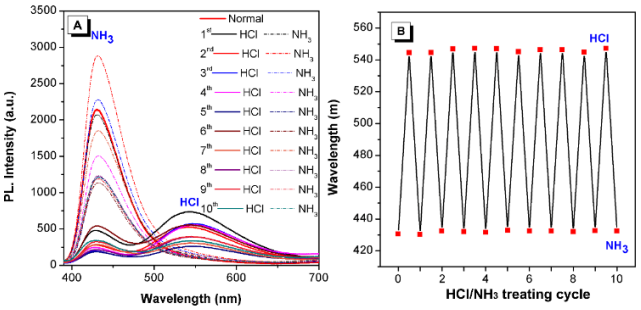

Figure 8. The pH-dependent fluorescence spectra of **Q-2Ph**.

Conclusions

Herein, three novel quinoxaline-based blue emitters, namely **Q-1-Py**, **Q-2-Py**, and **Q-2Ph**, in which the quinoxaline acts as an electron-withdrawning group and the pyrene (or diphenyl) moieties as electron donors, were synthesized by a Pd-catalysed Suzuki coupling reaction. Due to the position-dependant substitution effect leading to steric hindrance, the compounds displayed distinguishable optical behavior. All of the compounds emitted deep blue to sky-blue emission in solution with considerable quantum yield depending on the subsitution position. The compounds **Q-1-Py**, **Q-2-Py**, and **Q-2Ph** were blue emitters with both ICT plus AIEE characteristics in the highly polar THF/H_2O mixture, and displayed typical AIEE characteristics in less polar solvents. Furthermore, the selected quinoxaline-based deep blue emitter **Q-2Ph** in doped devices exhibited deep blue EL (428 nm) with CIE coordinates of (x = 0.15, y = 0.06). Moreover, the compound **Q-2Ph**, containing a quinoxaline unit, acts as a ratiometric gas sensor for detecting the presence of HCl and NH_3 vapor through conversion-emission behavior from blue to yellow. Thus, the newly designed quinoxaline-based compounds not only enrich the AIE lumingous family, but also provide more diverse deep blue emitters with AIE characteristics as multifunctional organic materials for blue OLED device applications.

Experimental

Materials: Unless otherwise stated, all reagents used were purchased from commercial sources and were used without further purification. Tetrahydrofuran was distilled prior to use. Pyrene-2-diboronic acid bis(pinacol) ester was prepared as described previously.[54]

Characterization

^{1}H and ^{13}C NMR spectra (400 MHz) were recorded on a Bruker AV 400 spectrometer using chloroform-*d* solvent and tetramethylsilane as internal reference. *J*-values are given in Hz. High-resolution mass spectra (HRMS) were taken on a LC/MS/MS, which consisted of a HPLC system (Ultimate 3000 RSLC, Thermo Scientific, USA) and a Q Exactive Orbitrap mass spectrometer. PL spectra were recorded on a Hitachi F-4700 spectrofluorometer. UV-vis absorption spectra were obtained on a Milton Ray Spectrofluorometer. PL quantum yields were measured using absolute methods. The cyclic voltammetry was carried out in 0.10 M tetrabutylammonium perchlorate in anhydrous dichloromethane and THF at a scan rate of 100 mVs^{-1} at room temperature. Thermogravimetric analysis was carried on a TA TGA Q5500 under dry nitrogen at a heating rate of 10°C/min. Thermal transitions were investigated by differential scanning calorimetry using a TA DSC Q1000 under dry nitrogen at a heating rate of 10 °C/min. The quantum chemistry calculations were performed on the Gaussian 16W (Rev A.03) (B3LYP/6–31G* basis set) software package.[55]

X-ray Crystallography

Crystallographic data of the compounds were collected on either a Rigaku 007HF equipped with Varimax confocal mirrors, an AFC11 goniometer and HyPix 6000 detector diffractometer in the case of **Q-1-Py** and **Q-2-Py**, or a Bruker D8 Venture diffractometer equipped with a CMOS detector and Triumph curved graphite monochromator. Cu Kα radiation (λ = 1.54178 Å) was employed in all cases and data sets were corrected for absorption and Lp effects.[56-57] The structures were solved by a charge flipping algorithm and refined by full-matrix least-squares methods on F^2.[58-60] In **Q-1-Py**, the hexane molecule of crystallization occupancy factor was allowed to refine freely which gave an occupancy of 58.2(5)% suggestive of some de-solvation. Further details are provided in Table S1 in the SI. CCDC 2050993-5 contain the supplementary crystallographic data for this paper. These data can be obtained free of charge from The Cambridge Crystallographic Data Centre via www.ccdc.cam.ac.uk/structures.

Synthesis of Pyrene-2-diboronic acid bis(pinacol) ester

To a 100 mL two-necked flask was added pyrene (2.00 g, 9.9 mmol, 1.0 eq.), bis(pinacolato)diboron (2.17 g, 8.55 mmol, 0.99 eq.), (1,5-cyclooctadiene)(methoxy)iridium(I) dimer (164 mg, 0.25 mmol, 0.025 eq.) and 4,4-di-*tert*-butyl-2,2'-dipyridyl (178 mg, 0.5 mmol, 0.05 eq.). The reaction mixture was degassed with nitrogen for 5 min, and then cyclohexane (30 mL) was added and the system refluxed at 80°C for 16 h. The reaction mixture was cooled to room temperature, and extracted with dichloromethane three times, and the combined extracts were washed with water and brine, dried with $MgSO_4$ and evaporated. The residue was purified by column chromatography with *n*-hexane/dichloromethane = 1:1 (v/v) to yield 1-boric acid pyrene (1.1 g, 34%) as a colorless solid.

Synthesis of 6,7-dibromo-2,3-diphenylquinoxaline

To a 100 mL two-necked flask was added 1,2-diphenyl-2,3-ethanedione (430 mg, 2.05 mmol, 1.0 eq.) and 4,5-dibromobenzene-1,2-diamine (540 mg, 2.03 mmol, 0.99 eq.). The reaction mixture was degassed with nitrogen for 5 min, and the acetic acid (10 ml) was added and the system was refluxed at 140 °C for 24 h. The reaction mixture was cooled to room temperature, and the product was washed three times with ethanol to yield 6,7-dibromo-2,3-diphenylquinoxaline (829 mg, 85%) as a yellow solid. This intermediate product was used directly without further purification due to the low solubility in common solvents.

Synthesis of Q-1-Py, Q-2-Py and Q-2Ph

A general procedure for the synthesis of **Q-1-Py**, **Q-2-Py**, and **Q-2Ph** is given here. To a 100 mL two-necked flask was added 6,7-dibromo-2,3-diphenylquinoxaline (0.91 mmol, 1.0 eq.), pyren-1-ylboronic acid (2.27 mmol, 2.5 eq.), potassium carbonate (2.18 mmol, 2.4 eq.), water (5 mL), ethanol (5 mL) and toluene (10 mL). The reaction mixture was degassed with nitrogen for 5 min, and tetrakis-triphenylphosphine palladium (0.09 mmol, 0.1 eq.) was added and the system was refluxed at 90°C for 24 h. Then the reaction mixture was cooled to room temperature and extracted with dichloromethane three times. The combined extracts were washed with water and brine, dried with dry $MgSO_4$ and evaporated. The residue was purified by column chromatography using CH_2Cl_2/hexane mixture as eluent to give a mixture of *anti*- and *syn*- isomers of the target compound 2,3-diphenyl-6,7-di(pyren-1-yl)quinoxaline (**Q-1-Py)** in the ratio of 2:1 (NMR analysis) as a light-yellow solid (251 mg, 38%). Melting point: undetectable. ^{1}H NMR (400 MHz, $CDCl_3$) δ 8.57 (s, 1H), 8.56 (s, 2H), 8.36 (d, *J* = 9.3 Hz, 2H), 8.24 (dd, *J* = 8.6, 5.5 Hz, 1H), 8.22 – 8.18 (m, 3H), 8.17 – 8.12 (m, 3H), 8.10 (d, *J* = 9.3 Hz, 2H), 8.05 – 8.00 (m, 3H), 7.98 (d, *J* = 5.8 Hz, 1H), 7.96 – 7.88 (m, 6H), 7.88 – 7.81 (m, 3H), 7.78 (d, *J* = 8.9 Hz, 2H), 7.74 (d, *J* = 9.3 Hz, 1H), 7.64 (ddd, *J* = 8.5, 7.8, 6.4 Hz, 6H), 7.57 (d, *J* = 8.0 Hz, 2H), 7.50 (d, *J* = 7.9 Hz, 2H), 7.42 – 7.35 (m, 9H). ^{13}C NMR (101 MHz, $CDCl_3$) δ 154.38, 154.27, 143.97, 143.81, 140.47, 140.29, 139.12, 135.45, 135.31, 132.52, 131.36, 131.18, 131.00, 130.71, 130.78, 130.38, 130.03, 129.36, 129.16, 128.72, 128.51, 127.95, 127.80, 127.42, 127.28, 126.12, 125.83, 125.43, 125.35, 125.12, 124.99, 124.79, 124.58, 124.16, 123.98 ppm. HRMS (FTMS+p ESI) *m/z*: calcd for $C_{52}H_{30}N_2$ 682.2409; found, 683.2482 $[M+H]^+$.

Q-2-Py: The residue was further recrystallized from a solution of dichloromethane and hexane to achieve 2,3-diphenyl-6,7-di(pyren-2-yl)quinoxaline (**Q-2-Py**) (285 mg, 61%). Melting point: 324 °C. ^{1}H NMR (400 MHz, $CDCl_3$): δ 8.57 (s, 2H), 8.13 (s, 4H), 8.08 (d, *J* = 7.6 Hz, 4H), 7.96 – 7.87 (m, 6H), 7.76 (d, *J* = 9.0 Hz, 4H), 7.63 (dd, *J* = 7.4, 1.9 Hz, 4H), 7.39 ppm (t, *J* = 5.7 Hz,

(FTMS+p ESI) *m/z*: calcd for $C_{52}H_{30}N_2$, 682.2409; found, 683.2481 $[M+H]^+$.

Q-2Ph: The residue was recrystallized from a solution of dichloromethane and hexane to afford 9,9'-((2,3-diphenylquinoxaline-6,7-diyl) bis(4,1-phenylene)) bis(9H-carbazole) **(Q-2Ph)** (210 mg, 60%). Melting point: 296 °C. ^{1}H NMR (400 MHz, $CDCl_3$) δ 8.30 (s, 2H), 7.62 (d, *J* = 7.5 Hz, 4H), 7.59 – 7.51 (m, 8H), 7.43 (t, *J* = 7.6 Hz, 4H), 7.40 – 7.29 (m, 12H). ^{13}C NMR (101 MHz, $CDCl_3$) δ 153.87, 142.95, 140.59, 140.46, 139.94, 139.33, 139.15, 130.40, 129.89, 128.88, 128.80, 128.31, 127.42, 127.02, 126.80 ppm. HRMS (ESI) *m/z*: calcd for $C_{44}H_{30}N_2$ 586.2409; found, 587.2483 $[M+H]^+$.

Supporting Information

The supporting information for this article is available on the WWW under https://doi.org/10.1002/cjoc.2021xxxxx.

Acknowledgement

X. M and F. X. contributed equally to this work. This work was supported by the National Natural Science Foundation of China (21975054 and 21602014), Natural Science Foundation of Guangdong Province of China (2019A1515010925), Guangdong Provincial Key Laboratory of Information Photonics Technology (2020B121201011), "One Hundred Talents Program" of the Guangdong University of Technology (GDUT) (1108-220413205), Guangdong provincial key laboratory of functional soft condensed matter of the Guangdong University of Technology (GDUT) (220413205). We also acknowledge the UK EPSRC National Crystallography Service at the University of Southampton for collecting X-ray diffraction data for **Q-1-Py** and **Q-2-Py**. CR thanks the EPSRC for an Overseas Travel grant (EP/R023816/1).

References

2[1] Freudenberg, J.; Jansch, D.; Hinkel, F.; Bunz, U. H. F. Immobilization Strategies for Organic Semiconducting Conjugated Polymers. *Chem. Rev.* **2018,** *118*, 5598-5689.
2[2] Kuehne, A. J.; Gather, M. C. Organic Lasers: Recent Developments on Materials, Device Geometries, and Fabrication Techniques. *Chem. Rev.* **2016,** *116*, 12823-12864.
2[3] Zhang, D. W.; Li, M.; Chen, C. F. Recent advances in circularly polarized electroluminescence based on organic light-emitting diodes. *Chem. Soc. Rev.* **2020,** *49*, 1331-1343.
2[4] Wang, Y.; Sun, L.; Wang, C.; Yang, F.; Ren, X.; Zhang, X.; Dong, H.; Hu, W. Organic crystalline materials in flexible electronics. *Chem. Soc. Rev.* **2019,** *48*, 1492-1530.
2[5] Yao, H.; Ye, L.; Zhang, H.; Li, S.; Zhang, S.; Hou, J. Molecular Design of Benzodithiophene-Based Organic Photovoltaic Materials. *Chem. Rev.* **2016,** *116*, 7397-457.
2[6] Huang, H.; Yang, L.; Facchetti, A.; Marks, T. J. Organic and Polymeric Semiconductors Enhanced by Noncovalent Conformational Locks, *Chem. Rev*. **2017**, *117*, 10291-10318.
2[7] Sun, J.; Zhu, P.; Wang, X.; Ji, J.; Habimana, J. D.; Shao, J.; Lei, H.; Zhang, Y.; Sun, X. Cell Based-Green Fluorescent Biosensor Using Cytotoxic Pathway for Bacterial Lipopolysaccharide Recognition. *J. Agric. Food Chem.* **2018,** *66*, 6869-6876.
2[8] Li, H.; Shi, W.; Song, J.; Jang, H. J.; Dailey, J.; Yu, J.; Katz, H. E. Chemical and Biomolecule Sensing with Organic Field-Effect Transistors. *Chem. Rev.* **2019,** *119*, 3-35.
2[9] Liras, M.; Barawi, M.; de la Pena O'Shea, V. A. Hybrid materials based on conjugated polymers and inorganic semiconductors as photocatalysts: from environmental to energy applications. *Chem. Soc. Rev.* **2019,** *48*, 5454-5487.
2[10] Zhang, X.; Gong, C.; Akakuru, O. U.; Su, Z.; Wu, A.; Wei, G. The design and biomedical applications of self-assembled two-dimensional organic biomaterials. *Chem. Soc. Rev.* **2019,** *48*, 5564-5595.
2[11] Hu, R.; Liu, T.; Zhang, X. B.; Huan, S. Y.; Wu, C.; Fu, T.; Tan, W. Multicolor fluorescent biosensor for multiplexed detection of DNA. *Anal. Chem.* **2014,** *86*, 5009-16.
2[13] Feng, X.; Xu, Z.; Hu, Z.; Qi, C.; Luo, D.; Zhao, X.; Mu, Z.; Redshaw, C.; Lam, J. W. Y.; Ma, D.; Tang, B. Z. Pyrene-based blue emitters with aggregation-induced emission features for high-performance organic light-emitting diodes. *J. Mater. Chem. C* **2019,** *7*, 2283-2290.
2[14] Yang, J.; Li, L.; Yu, Y.; Ren, Z.; Peng, Q.; Ye, S.; Li Q.; Li, Zhen. Blue pyrene-based AIEgens: inhibited intermolecular π–π stacking through the introduction of substituents with controllable intramolecular conjugation, and high external quantum efficiencies up to 3.46% in non-doped OLEDs, ***Mater. Chem. Front.***, 2017,**1**, 91-99.
2[15] Mei, J.; Leung, N. L.; Kwok, R. T.; Lam, J. W.; Tang, B. Z. Aggregation-Induced Emission: Together We Shine, United We Soar! *Chem. Rev.* **2015,** *115*, 11718-940.
2[16] Zhao, Q.; Zhang, X. A.; Wei, Q.; Wang, J.; Shen, X. Y.; Qin, A.; Sun, J. Z.; Tang, B. Z. Tetraphenylethene modified perylene bisimide: effect of the number of substituents on AIE performance. *Chem. Commun.* **2012,** *48*, 11671-3.
2[17] Luo, J.; Xie, Z.; Lam, J. W.; Cheng, L.; Chen, H.; Qiu, C.; Kwok, H. S.; Zhan, X.; Liu, Y.; Zhu, D.; Tang, B. Z. Aggregation-induced emission of 1-methyl-1,2,3,4,5-pentaphenylsilole. *Chem. Commun.* **2001,** 1740-1.
2[18] Yuan, W. Z.; Lu, P.; Chen, S.; Lam, J. W.; Wang, Z.; Liu, Y.; Kwok, H. S.; Ma, Y.; Tang, B. Z. Changing the behavior of chromophores from aggregation-caused quenching to aggregation-induced emission: development of highly efficient light emitters in the solid state. *Adv. Mater.* **2010,** *22*, 2159-63.
2[19] Yang, J.; Chi, Z.; Zhu, W.; Tang, B. Z.; Li, Z. Aggregation-induced emission: a coming-of-age ceremony at the age of eighteen. *Sci. China Chem*, 2019, 62, 1090-1098.
2[20] Xu, Z.; Tang, B. Z.; Wang, Y.; Ma, D. Recent advances in high performance blue organic light-emitting diodes based on fluorescence emitters. *J. Mater.Chem. C* **2020,** *8*, 2614-2642.
2[21] Han, P.; Lin, C.; Ma, D.; Qin, A.; Tang, B. Z. Violet-Blue Emitters Featuring Aggregation-Enhanced Emission Characteristics for Nondoped OLEDs with CIEy Smaller than 0.046. *ACS Appl. Mater. Interfaces* **2020,** *12*, 46366-46372.
2[22] Wang, J.; Gu, X.; Zhang, P.; Huang, X.; Zheng, X.; Chen, M.; Feng, H.; Kwok, R. T. K.; Lam, J. W. Y.; Tang, B. Z. Ionization and Anion-pi(+) Interaction: A New Strategy for Structural Design of Aggregation-Induced Emission Luminogens. *J. Am. Chem. Soc.* **2017,** *139*, 16974-16979.
2[23] Sasaki, S.; Suzuki, S.; Sameera, W. M.; Igawa, K.; Morokuma, K.; Konishi, G. Highly Twisted N,N-Dialkylamines as a Design Strategy to Tune Simple Aromatic Hydrocarbons as Steric Environment-Sensitive Fluorophores. *J. Am. Chem. Soc.* **2016,** *138*, 8194-206.
2[24] Chen, M.; Chen, R.; Shi, Y.; Wang, J.; Cheng, Y.; Li, Y.; Gao, X.; Yan, Y.; Sun, J. Z.; Qin, A.; Kwok, R. T. K.; Lam, J. W. Y.; Tang, B. Z. Malonitrile-Functionalized Tetraphenylpyrazine: Aggregation-Induced Emission, Ratiometric Detection of Hydrogen Sulfide, and Mechanochromism. *Adv. Funct. Mater.* **2017,** *28*, 1704689.
2[25] Chen, M.; Li, L.; Nie, H.; Shi, Y.; Mei, J.; Wang, J.; Sun, J. Z.; Qin, A.; Tang, B. Z. N-type pyrazine and triazole-based luminogens with aggregation-enhanced emission characteristics. *Chem. Commun.* **2015,** *51*, 10710-10713.
2[26] Li, J.; Wang, J.; Li, H.; Song, N.; Wang, D.; Tang, B. Z. Supramolecular materials based on AIE luminogens (AIEgens): construction and applications. *Chem. Soc. Rev.* **2020,** *49*, 1144-1172.
2[27] Chen, M.; Li, L.; Nie, H.; Tong, J.; Yan, L.; Xu, B.; Sun, J. Z.; Tian, W.; Zhao, Z.; Qin, A.; Tang, B. Z. Tetraphenylpyrazine-based AIEgens: facile preparation and tunable light emission. *Chem. Sci.* **2015,** *6*, 1932-1937.
2[28] Chen, M.; Hu, X.; Liu, J.; Li, B.; Leung, N. L. C.; Viglianti, L.; Cheung, T. S.; Sung, H. H. Y.; Kwok, R. T. K.; Williams, I. D.; Qin, A.; Lam, J. W. Y.; Tang, B. Z. Rational design of red AIEgens with a new core structure from non-emissive heteroaromatics. *Chem. Sci.* **2018,** *9*, 7829-7834.
2[29] Zhang, M.; Dai, Z. C.; Qian, S. S.; Liu, J. Y.; Xiao, Y.; Lu, A. M.; Zhu, H. L.; Wang, J. X.; Ye, Y. H. Design, synthesis, antifungal, and antioxidant activities of (E)-6-((2-phenylhydrazono)methyl)quinoxaline derivatives. *J. Agric. Food Chem.* **2014,** *62*, 9637-43.
2[30] Son, H. J.; Han, W. S.; Yoo, D. H.; Min, K. T.; Kwon, S. N.; Ko, J.; Kang, S. O. Fluorescence control on panchromatic spectra via c-alkylation on arylated quinoxalines. *J. Org. Chem.* **2009,** *74*, 3175-8.
2[31] Rajeswara, R. M.; Liao, C.-W.; Su, W.-L.; Sun, S.-S. Quinoxaline based D–A–D molecules: high contrast reversible solid-state mechano- and thermo-responsive fluorescent materials. *J. Mater.Chem. C* **2013,** *1*, 5491-5501.
2[32] Pashazadeh, R.; Pander, P.; Lazauskas, A.; Dias, F. B.; Grazulevicius, J. V. Multicolor Luminescence Switching and Controllable Thermally Activated Delayed Fluorescence Turn on/Turn off in Carbazole-Quinoxaline-Carbazole Triads. *J. Phys. Chem. Lett.* **2018,** *9*,

1172-1177.
2[33] Pashazadeh, R.; Sych, G.; Nasiri, S.; Leitonas, K.; Lazauskas, A.; Volyniuk, D.; Skabara, P. J.; Grazulevicius, J. V. Multifunctional asymmetric D-A-D' compounds: Mechanochromic luminescence, thermally activated delayed fluorescence and aggregation enhanced emission. *Chem. Eng. J.* **2020,** *401*, 125962.
2[34] Pashazadeh, R.; Pander, P.; Bucinskas, A.; Skabara, P. J.; Dias, F. B.; Grazulevicius, J. V. An iminodibenzyl-quinoxaline-iminodibenzyl scaffold as a mechanochromic and dual emitter: donor and bridge effects on optical properties. *Chem. Commun.* **2018,** *54*, 13857-13860.
2[35] Wang, C.-Z.; Noda, Y.; Wu, C.; Feng, X.; Venkatesan, P.; Cong, H.; Elsegood, M. R. J.; Warwick, T. G.; Teat, S. J.; Redshaw, C.; Yamato, T. Multiple Photoluminescence from Pyrene-Fused Hexaarylbenzenes with Aggregation-Enhanced Emission Features. *Asian J. Org. Chem.* **2018,** *7*, 444-450.
2[36] Li, Q.; Li, Z. Molecular Packing: Another Key Point for the Performance of Organic and Polymeric Optoelectronic Materials, *Acc. Chem. Res.* **2020**, *53*, 962–973.
2[37] Yang, J.; Fang, M.; Li, Z.; Organic luminescent materials: The concentration on aggregates from aggregation-induced emission, *Aggregate*, **2020**, *1*, 6-18.
2[38] Chang, K.; Li, Q.; Li, Z. Advances in Mechanoluminescence and Its Applications. *Chin. J. Org. Chem.* **2020**, *40*, 3656-3671.
2[39] Crawford, A. G.; Dwyer, A. D.; Liu, Z.; Steffen, A.; Beeby, A.; Palsson, L. O.; Tozer, D. J.; Marder, T. B. Experimental and theoretical studies of the photophysical properties of 2- and 2,7-functionalized pyrene derivatives. *J. Am. Chem. Soc.* **2011,** *133*, 13349-62.
2[40] Islam, M. M.; Hu, Z.; Wang, Q.; Redshaw, C.; Feng, X. Pyrene-based aggregation-induced emission luminogens and their applications. *Mater. Chem. Front.* **2019,** *3*, 762-781.
2[41] Wang, Q.; Gao, W.; Chen, Y.; Wang, X.; Zeng, J.; Liu, Y.; Ran, H.; Hu, Z.; Bai, J.; Feng, X.; Redshaw, C.; Chen, Q.; Hu, J. Y. Pyrene-fused Dibenzoazatetracenes: Synthesis, Crystal Structures, Photophysical Properties and their Morphologies. *Asian J. Org. Chem.* **2020,** *10*, 233-240.
2[42] Wang, C. Z.; Ichiyanagi, H.; Sakaguchi, K.; Feng, X.; Elsegood, M. R. J.; Redshaw, C.; Yamato, T. Pyrene-Based Approach to Tune Emission Color from Blue to Yellow. *J. Org. Chem.* **2017,** *82*, 7176-7182.
2[43] Feng, X.; Hu, J. Y.; Redshaw, C.; Yamato, T. Functionalization of Pyrene To Prepare Luminescent Materials-Typical Examples of Synthetic Methodology. *Chem. Eur. J.* **2016,** *22*, 11898-916.
2[44] Yang, S. W.; Elangovan, A.; Hwang, K. C.; Ho, T. I. Electronic polarization reversal and excited state intramolecular charge transfer in donor/acceptor ethynylpyrenes. *J. Phys. Chem. B* **2005,** *109*, 16628-35.
2[45] Sung, J.; Kim, P.; Lee, Y. O.; Kim, J. S.; Kim, D. Characterization of Ultrafast Intramolecular Charge Transfer Dynamics in Pyrenyl Derivatives: Systematic Change of the Number of Peripheral N,N-Dimethyaniline Substituents. *J. Phys. Chem. Lett.* **2011,** *2*, 818-823.
2[46] Dong, Y.; Lam, J. W. Y.; Qin, A.; Sun, J.; Liu, J.; Li, Z.; Sun, J.; Sung, H. H. Y.; Williams, I. D.; Kwok H. S.; Tang, B. Z. Aggregation-induced and crystallization-enhanced emissions of 1,2-diphenyl-3,4-bis(diphenylmethylene)-1-cyclobutene, *Chem. Commun.* **2007**, 3255-3257.
2[47] Qin, W.; Li, K.; Feng, G.; Li, M.; Yang, Z.; Liu, B.; Tang, B. Z. Bright and Photostable Organic Fluorescent Dots with Aggregation-Induced Emission Characteristics for Noninvasive Long-Term Cell Imaging. *Adv. Funct. Mater.* **2014,** *24*, 635-643.
2[48] Qin, W.; Ding, D.; Liu, J.; Yuan, W. Z.; Hu, Y.; Liu, B.; Tang, B. Z. Bioimaging: Biocompatible Nanoparticles with Aggregation-Induced Emission Characteristics as Far-Red/Near-Infrared Fluorescent Bioprobes for in Vitro and In Vivo Imaging Applications (Adv. Funct. Mater. 4/2012). *Adv. Funct. Mater.* **2012,** *22*, 665-665.
2[49] Bhattacharyya, A.; Guchhait, N. Intriguing photophysical aspects of nitro substituted 2-(2'-hydroxyphenyl)benzothiazole (HBT) derivative: AIE in non-polar media? *Chem. Phy.* **2021**, 541, 111032.
2[50] Wang, E.; Lam, J. W. Y.; Hu, R.; Zhang, C.; Zhao, Y. S.; Tang, B. Z. Twisted intramolecular charge transfer, aggregation-induced emission, supramolecular self-assembly and the optical waveguide of barbituric acid-functionalized tetraphenylethene. *J. Mater.Chem. C* **2014,** *2,* 1801-1807.
2[51] Alam, P.; Leung, N. L. C.; Su, H.; Qiu, Z.; Kwok, R. T. K.; Lam, J. W. Y.; Tang, B. Z. A Highly Sensitive Bimodal Detection of Amine Vapours Based on Aggregation Induced Emission of 1,2-Dihydroquinoxaline Derivatives. *Chem. Eur. J.* **2017,** *23*, 14911-14917.
2[52] Liu, D.; Zhang, Z.; Zhang, H.; Wang, Y. A novel approach towards white photoluminescence and electroluminescence by controlled protonation of a blue fluorophore. *Chem. Commun.* **2013,** *49*, 10001-3.
2[53] He, Y.; Li, Y.; Su, H.; Si, Y.; Liu, Y.; Peng, Q.; He, J.; Hou, H.; Li, K. An o-phthalimide-based multistimuli-responsive aggregation-induced emission (AIE) system. *Mater. Chem. Front.* **2019,** *3*, 50-56.
2[54] Coventry, D. N.; Batsanov, A. S.; Goeta, A. E.; Howard, J. A.; Marder, T. B.; Perutz, R. N. Selective Ir-catalysed borylation of polycyclic aromatic hydrocarbons: structures of naphthalene-2,6-bis(boronate), pyrene-2,7-bis(boronate) and perylene-2,5,8,11-tetra(boronate) esters. *Chem. Commun.* **2005,** , 2172-4.
2[55] Frisch, M. J. et al. Gaussian 03, Revision C.02, Gaussian, Inc., Wallingford, CT, 2004.
2[56] SAINT and APEX 2. Software for CCD diffractometers. **2015**.
2[57] Sheldrick, G. M. A short history of SHELX. *Acta Crystallogr. A* **2008,** *64* (Pt 1), 112-22.
2[58] Sheldrick, G. M. SHELXT - integrated space-group and crystal-structure determination. *Acta Crystallogr A Found Adv* **2015,** *71*, 3-8.
2[59] Westrip, S. P. publCIF: software for editing, validating and formatting crystallographic information files. *J. Appl. Crystallogr.* **2010,** *43*, 920-925.
2[60] Zhang, J.; Ma, X. F.; Xuan, X. P. Disordered Fragments of Chemical Structures Based on Single-crystal X-ray Diffraction. *Chinese J. Struct. Chem.* **2020**, *39*, 698-708.

(The following will be filled in by the editorial staff)

Manuscript received: XXXX, 2021
Manuscript revised: XXXX, 2021
Manuscript accepted: XXXX, 2021
Accepted manuscript online: XXXX, 2021
Version of record online: XXXX, 2021

New Quinoxaline-Based Blue Emitters: Molecular Structures, Aggregation-Induced Enhanced Emission Characteristics and OLED Application

Xiaoyu Mao,[#a] Fuli Xie,[#b] Xiaohui Wang,[a] Qingsong Wang,[a] Zhipeng Qiu,[c] Mark R. J. Elsegood,[d] Jie Bai,[a] Xing Feng,[*,a] Carl Redshaw,[e] Yanping Huo,[*,c] Jian-Yong Hu,[*,b] Qing Chen[*,f]

Chin. J. Chem. **2021**, *39*, XXX—XXX. **DOI: 10.1002/cjoc.202100XXX**

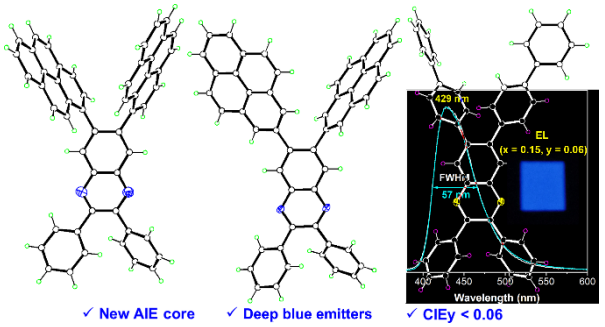

New deep blue light emitters, containing quinoxaline and pyrene (biphenyl) moieties are presented, which display both intramolecular charge transfer and aggregation-induced emission characteristics. More importantly, the selected blue emitter gives a deep blue electroluminescence (EL) peak at 428 nm with a narrow FWHM of 57 nm in doped OLED devices, and the Commission Internationale de L'Eclairage (CIE) chromaticity coordinate of (0.15, 0.06).

